the FEBS Journal

Oncogenic mutations weaken the interactions that stabilize the p110α-p85α heterodimer in phosphatidylinositol 3-kinase α

Ignacia Echeverria[1,2,3], Yunlong Liu[3], Sandra B. Gabelli[3,4] and L. Mario Amzel[3]

1 Department of Bioengineering and Therapeutic Sciences, School of Pharmacy, University of California at San Francisco, CA, USA
2 Department of Pharmaceutical Chemistry, School of Pharmacy, University of California at San Francisco, CA, USA
3 Department of Biophysics and Biophysical Chemistry, Johns Hopkins University School of Medicine, Baltimore, MD, USA
4 Departments of Medicine and Oncology, Johns Hopkins University School of Medicine, Baltimore, MD, USA

Keywords
allostery; molecular dynamics simulations; normal mode analysis; oncogenic mutations; phosphatidylinositol 3-kinase activation

Correspondence
L. M. Amzel, Department of Biophysics and Biophysical Chemistry, Johns Hopkins University School of Medicine, 725 N. Wolfe St., 606 WBSB, Baltimore, MD 21205, USA
Fax: 1-410-955-0637
Tel: 1-410-955-3955
E-mail: mamzel@jhmi.edu

(Received 16 April 2015, revised 20 June 2015, accepted 26 June 2015)

doi:10.1111/febs.13365

Phosphatidylinositol 3-kinase (PI3K) α is a heterodimeric lipid kinase that catalyzes the conversion of phosphoinositol-4,5-bisphosphate to phosphoinositol-3,4,5-trisphosphate. The PI3Kα signaling pathway plays an important role in cell growth, proliferation, and survival. This pathway is activated in numerous cancers, where the *PI3KCA* gene, which encodes for the p110α PI3Kα subunit, is mutated. Its mutation often results in gain of enzymatic activity; however, the mechanism of activation by oncogenic mutations remains unknown. Here, using computational methods, we show that oncogenic mutations that are far from the catalytic site and increase the enzymatic affinity destabilize the p110α–p85α dimer. By affecting the dynamics of the protein, these mutations favor the conformations that reduce the autoinhibitory effect of the p85α nSH2 domain. For example, we determined that, in all of the mutants, the nSH2 domain shows increased positional heterogeneity as compared with the wild-type, as demonstrated by changes in the fluctuation profiles computed by normal mode analysis of coarse-grained elastic network models. Analysis of the interdomain interactions of the wild-type and mutants at the p110α–p85α interface obtained with molecular dynamics simulations suggest that all of the tumor-associated mutations effectively weaken the interactions between p110α and p85α by disrupting key stabilizing interactions. These findings have important implications for understanding how oncogenic mutations change the conformational multiplicity of PI3Kα and lead to increased enzymatic activity. This mechanism may apply to other enzymes and/or macromolecular complexes that play a key role in cell signaling.

Introduction

Phosphatidylinositol 3-kinases (PI3Ks) are a family of lipid kinases that initiate signaling cascades that control a variety of cellular functions, including cell growth, proliferation, motility, survival, and intracellular trafficking [1]. These enzymes catalyze a simple but important reaction: they phosphorylate the 3-hydroxyl

Abbreviations
ABD, adaptor-binding domain; ENM, elastic network model; HDX-MS, hydrogen–deuterium exchange mass spectroscopy; iSH2, inter-Src homology 2; MD, molecular dynamics; NMA, normal mode analysis; nSASA, normalized solvent-accessible surface area; PDB, Protein Data Bank; PI3K, phosphatidylinositol 3-kinase; pTyr, phosphotyrosine; RTK, receptor tyrosine kinase; SASA, solvent-accessible surface area; SH2, Src homology 2; WT, wild-type.

position of the inositol ring of phosphatidylinositol-4,5-bisphosphate to yield phosphatidylinositol-3,4,5-trisphosphate [2]. Phosphatidylinositol-3,4,5-trisphosphate is recognized by proteins containing a pleckstrin homology domain that are recruited to the cell membrane, where they initiate signaling.

PI3K enzymes belong to different classes that differ in their structure and function [3]. (For a complete description of the PI3K enzyme classification, see [4].) PI3Kα, a class IA isoform, is a heterodimer consisting of a catalytic subunit (p110α) and a regulatory subunit (p85α) that binds receptor tyrosine kinases (RTKs) or other substrates that activate PI3K. Each PI3Kα subunit is composed of five domains (Fig. 1A,B). p110α comprises an adaptor-binding domain (ABD), a Ras-binding domain, a C2 domain, a helical domain, and a kinase domain. The last four domains have significant sequence homology among isoforms. p85α contains an Src homology 3 domain, a GTPase-activating protein (GAP-like or BH) domain, and two Src homology 2 (SH2) domains (nSH2 and cSH2) separated by an inter-SH2 (iSH2) domain. PI3Kα forms an obligate heterodimer in which p110α, which by itself is unstable in cells, is stabilized upon dimerization with p85α [5]. However, the nSH2 domain of p85α inhibits the basal kinase activity of p110α, suggesting that the activation mechanism of PI3Kα includes relief of this autoinhibition.

Physiological activation of PI3Kα is triggered by binding of phosphorylated RTKs or their accessory proteins, such as insulin receptor substrate 1 [3,6], that bridge the interaction between RTK and PI3Kα. These phosphorylated activators, by dislodging the nSH2 domain from its inhibitory interaction with the helical domain, relieve the nSH2 domain's partial inhibition of PI3Kα activity [6].

PIK3CA, the gene that encodes the p110α subunit, has been found to be mutated in 12% of all tumor sequences deposited in the catalog of mutations in cancers [7]. Mutations of *PIK3CA* in human cancers [8,9] are associated with increased enzymatic PI3Kα activity [10,11]. Cancer-associated mutations [12–14] have been reported throughout the sequence of p110α [15,16]. However, 'hot-spot' mutations are located mostly in the helical domain (Glu542 and Glu545) and the kinase domain (His1047). For example, of the 7548 unique mutations cataloged at the COSMIC database,

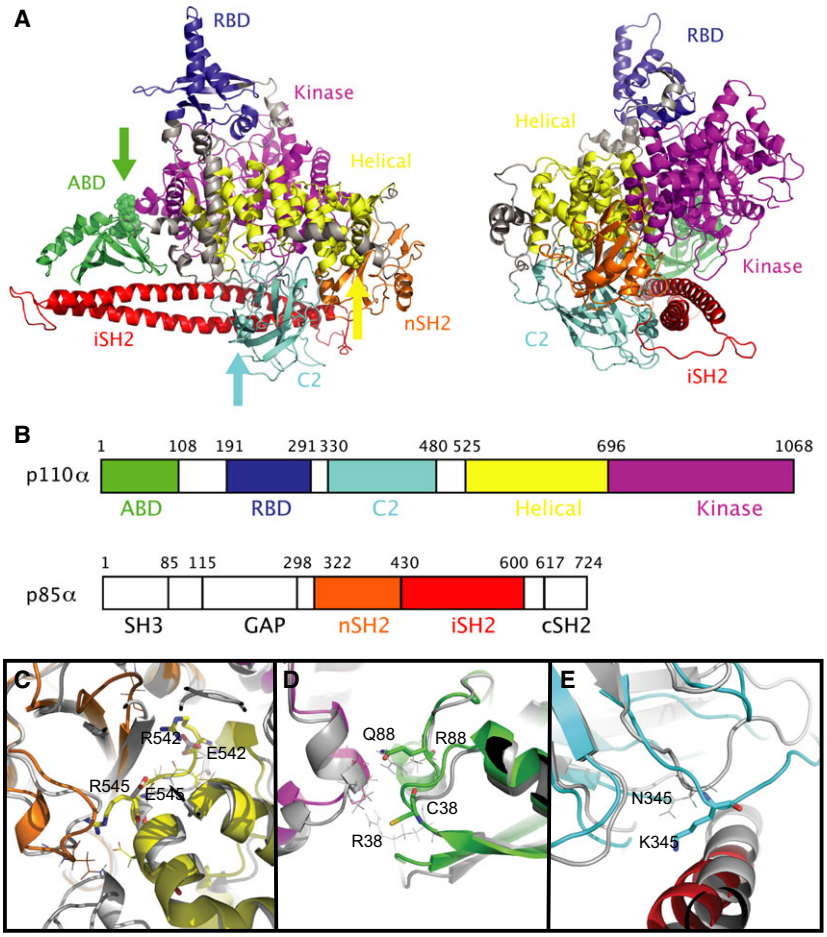

Fig. 1. Overview of the p110α–niSH2 heterodimer. (A) Ribbon diagram of the p110α–niSH2 heterodimer (front view and side view). Arrows indicate the positions of the studied mutations, which are shown in sphere representation. (B) Scheme of the domain organization. The same color coding is used throughout the figures, unless specified. Gray regions are linkers between domains. (C) The nSH2–helical domain interface where the E542R/E545R mutation was modeled. The WT is shown in gray. (D) The ABD–kinase domain interface where the R38C/R88Q mutation was modeled. The WT is shown in gray. (E) The C2–iSH2 domain interface where the N345K mutation was modeled. The WT is shown in gray. RBD, Ras-binding domain.

1687 (22%) correspond to His1047, 1153 (15%) to Glu545, and 758 (10%) to Glu542 [COSMIC database [7] (http://cancer.sanger.ac.uk/cosmic/gene/analysis?ln=PIK3CA#hist) as of March, 2015]. These mutations are known to activate PI3Kα by different mechanisms [16–18]. Mutations of Glu542 and Glu545 are located in the loop of the helical domain that contacts the nSH2 domain [16]. It has been suggested that, in the wild-type (WT), the interactions between the nSH2 and helical domains are such that they 'lock' PI3K in its inactive conformation, and that oncogenic mutations activate PI3Kα by weakening the interaction between the helical and nSH2 domains [10,11,16,18]. In contrast, the structure of the H1047R mutant [16] shows that R1047 adopts a conformation perpendicular to the orientation of H1047 in the WT, and two loops of the oncogenic mutant kinase domain contact the cell membrane. Biochemical assays have revealed that the enzymatic activity of the p110α H1047R mutant is more sensitive than that of the WT to the lipid membrane composition [16]. These findings suggest that the functional effect of the H1047R mutation is attributable to the change in the interaction between PI3Kα and the cellular membrane [19,20], increasing the lipid kinase activity by allowing easier access to the membrane-bound phosphoinositol-4,5-bisphosphate substrate [16]. Other common mutations that are also associated with enzyme activation are located in the ABD and the C2 domain [7], and their activation mechanism remains unknown [18,21,22].

Currently, several PI3K inhibitors are under development as possible cancer therapeutic agents [23–25]. However, as different PI3K isoforms have different biological functions, an effective PI3K inhibitor has to be isoform-selective to avoid side effects [26–28]. Furthermore, depending on the activation mechanism of the associated oncogenic mutation, it may be necessary to design mutant-specific inhibitors. Understanding the functional effects of somatic mutations on the activation and activity of PI3K is necessary to guide the design of these inhibitors.

A recent experimental study of the dynamics of WT and cancer-linked mutants of the p110α–p85α complex provided important information for understanding the dynamic effects of common oncogenic mutations. Using hydrogen–deuterium exchange mass spectroscopy (HDX-MS), Williams *et al.* determined that four distinct conformational events are associated with the activation of PI3Kα [22]: (a) disruption of the nSH2–helical interface; (b) disruption of the iSH2–C2 interface; (c) movement of the ABD relative to the kinase domain; and (d) interaction of the kinase domain with lipid. One or more of these four distinct events detected in the activation of WT p110α–p85α are thought to also activate the enzyme with cancer-related mutations. However, the HDX-MS studies can determine neither the order of these events, nor whether they are spatially or temporally correlated.

The molecular mechanism by which the structural and dynamic effects of different mutations are propagated throughout the PI3Kα structure and affect its activity cannot be directly inferred from structural and/or HDX-MS studies. On the basis of the available evidence, we hypothesize that PI3Kα becomes activated through dynamic changes in the relative conformations of the two subunits. If this is the case, the allosteric effects of PI3Kα mutations far from the active site that increase the enzymatic activity are associated with changes in the large-scale dynamic behavior of the protein: changes in the thermal fluctuation would facilitate allosteric changes in the kinase domain without large changes in the average structure of the other domains [29–32]. To probe this mechanism, we used computational methods to characterize changes in the interdomain interactions and their effects on the dynamics of WT and mutant PI3K. We explored the effects of five different oncogenic mutations, to elucidate the molecular mechanism by which oncogenic mutations lead to enzyme activation. This comprehensive computational investigation addresses the flexibility and dynamics of WT and mutant PI3Kα, and provides a basis for understanding how these properties affect PI3K activation. Normal mode analysis (NMA) with coarse-grained elastic network models (ENMs) and molecular dynamics (MD) simulations allowed assessment of the conformational fluctuations of the system over a range of timescales. On the basis of these results, we propose a model for the activation of PI3Kα by oncogenic mutations that involves allosteric communication between different parts of the proteins mediated by destabilization of the p110α–p85α dimer.

Results

Biochemical and cellular studies have shown that the oncogenic mutations studied here are associated with gain of enzymatic activity of PI3Kα [10,17]. It is also known that mutations in different p110α domains may activate PI3Kα by different mechanisms [16,17]. Nevertheless, these mutations have a common characteristic: they are located far from the catalytic site at the interface between different PI3Kα domains (Fig. 1A). For example, the helical domain mutations E542K and E545K are located at the interface between the helical domain of p110α and the nSH2 domain of p85α.

These mutations result in the displacement of one of the nSH2 domain β-sheets (residues 377–383), changing the interaction between the nSH2 domain and the helical domain (Fig. 1C). The ABD mutations R38C and R88Q, which are located at the interface of the ABD and the kinase domain (Fig. 1D) disrupt the interactions of Arg38 and Arg88 with Asp743 and Asp746 in the kinase domain. The C2 N345K mutation, located at the interface of the C2 and iSH2 domains (Fig. 1E), changes the conformation of the loop region where this residue is located. Overall, our results show that the analyzed mutations induce local perturbations at interfaces between PI3Kα domains. These models are in agreement with the experimental evidence showing that oncogenic mutations results in local structural changes [16], which we propose change the dynamics of the protein and result in the release of autoinhibition.

Oncogenic mutations increase the fluctuations of the nSH2 domain

The effects of the oncogenic mutations on the positional fluctuations of the different domains were studied by computing the elastic network normal modes (ENM) of WT and mutant proteins. ENMs constitute a powerful tool with which to study the inherent flexibility of the protein, from which conformational transitions can be inferred by identifying and characterizing the collective motions described by vibrational modes [33]. Figure 2 shows the characteristic fluctuation profile of every PI3Kα domain. ENM analysis of WT and mutant PI3Kαs showed that residue fluctuations and overall collective motions of the protein are affected by point mutations in the ABD, C2, and helical domains. Remarkably, all of these mutations significantly affect the fluctuation profile of the nSH2 domain of p85α subunit. Specifically, for all mutants, the nSH2 domain showed a significantly larger amplitude of movement (i.e. up to a three-fold increase in the average fluctuations) than the WT model (Fig. 2F), particularly in the region spanning residues 377–410. This segment includes the β-sheet and α-helix that face the interface between the nSH2 domain and the helical domain (Fig. 1C). In the case of the N345K mutant (C2 domain), the ABD domain and iSH2 domain become more rigid, particularly residues 506–524 of the iSH2 domain (Fig. 2G). These residues correspond to the coil region in the coiled-coil turn at the interface between the ABD and the iSH2 domain. No significant changes in the fluctuation profiles were observed for the C2 (Fig. 2C), helical (Fig. 2D) and kinase (Fig. 2E) domains. However, dynamic effects that are not detected by ENMs may be present. These results show that, regardless of where mutations are located, they all ultimately result in release of the autoinhibitory effect of the nSH2 domain. The molecular mechanism by which such an effect is transmitted along the protein was investigated with MD simulations.

Oncogenic mutations disrupt the interactions at the p110α–p85α interface

As already mentioned, all of the oncogenic mutations studied here are located at interfaces between domains. We studied the dynamic effects of these mutations by analyzing the residue-to-residue distances at the interfaces between the helical and nSH2 domains, the C2 and iSH2 domains and the ABD and the kinase domain in MD trajectories (see Experimental procedures). All mutations significantly change how the nSH2 and helical domains interact (Fig. 3). For example, the interaction between Glu542 (helical domain) and Leu380 (nSH2 domain) is conserved in all cases, even when residue 542 is mutated to lysine. On the other hand, the interaction between Asn542 (helical domain) and Ser361 (nSH2 domain) is lost in all mutants. The distance distribution for this interaction has two well-defined peaks, which correspond to direct protein–protein interactions and water-mediated interactions. The E542K/E545K mutation also disrupts the interaction between Glu545 (helical domain) and Lys379 (nSH2 domain). Additionally, the N345K and R38C/R88C mutations significantly change the distance distribution for helical domain residues Lys379, Ile381, and Lys382. These results support the notion that even distant mutations (R38C/R88Q, and N345K) effectively weaken the interaction between the nSH2 and helical domains, thus increasing the population of molecules in which the nSH2 domain is not inhibitory.

We also investigated the interaction between the C2 and iSH2 domains. In the WT, Asn345 (C2 domain) is within hydrogen bonding distance of Glu560 and Glu564 (iSH2 domain). These interactions are lost in the N345K mutant (Fig. 4). Surprisingly, these interactions are also lost in the structures with mutations in the helical domain and the ABD (Fig. 4). The fact that the E542K/E545K mutation (helical domain) has a significant effect in the C2–iSH2 interface suggests that weakening the nSH2–helical interface affects the overall dynamics of the subunit interaction in the PI3K heterodimer, resulting in significant effects far from the mutation sites. The R38C/R88Q mutation (ABD) also significantly disrupt the C2–iSH2 interface, for which we monitored the His450 to Tyr467 contact. All

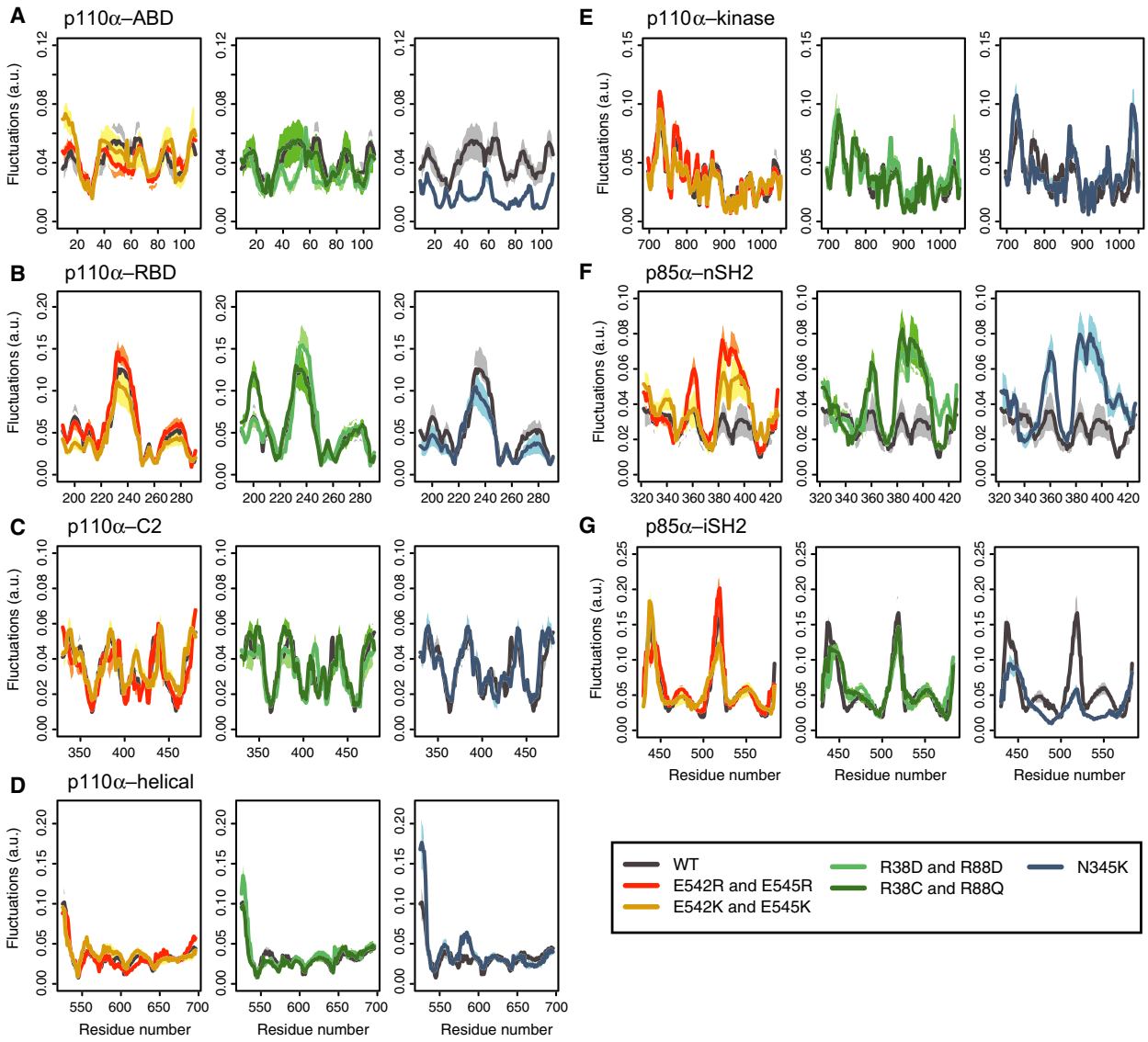

Fig. 2. Fluctuations of the p110α and p85α domains. The fluctuation profiles were obtained by generating random linear combinations of the first six vibrational modes, shown in arbitrary units (a.u.). Fluctuations of the WT protein are in gray in all plots for comparison. (A) Fluctuations of the ABD. (B) Fluctuations of the Ras-binding domain (RBD). (C) Fluctuations of the C2 domain. (D) Fluctuations of the helical domain. (E) Fluctuations of the kinase domain. (F) Fluctuations of the nSH2 domain. (G) Fluctuations of the iSH2 domain. Shaded areas correspond to one standard deviation of the fluctuations.

of our simulations showed that His450 (C2 domain) and Tyr467 (iSH2 domain) are ~ 3.4 Å apart (Fig. 4). His450 is located in a loop region of the C2 domain, and interacts via stacking interactions with Tyr467 of the iSH2 domain. This interaction is more prominent in the E542K/E545K (helical domain) and R38C/R88Q (ABD) mutants. Previous studies have suggested that disruption of the C2–iSH2 interface leads to enzyme activation [34]. These structural changes have also been detected in HDX-MS experiments, which suggests that disruption of this interface may occur upon membrane binding as part of the enzyme's catalytic cycle [19].

We also evaluated the interface between the ABD and the kinase domain. In the WT, Arg38 and Arg88 are at hydrogen bonding distance from Asp743 and Asp746, which are located in consecutive turns of the helices of the kinase domain. Upon mutation of Arg38 and Arg88, these interactions are disturbed (Fig. 5), and may affect the relationship

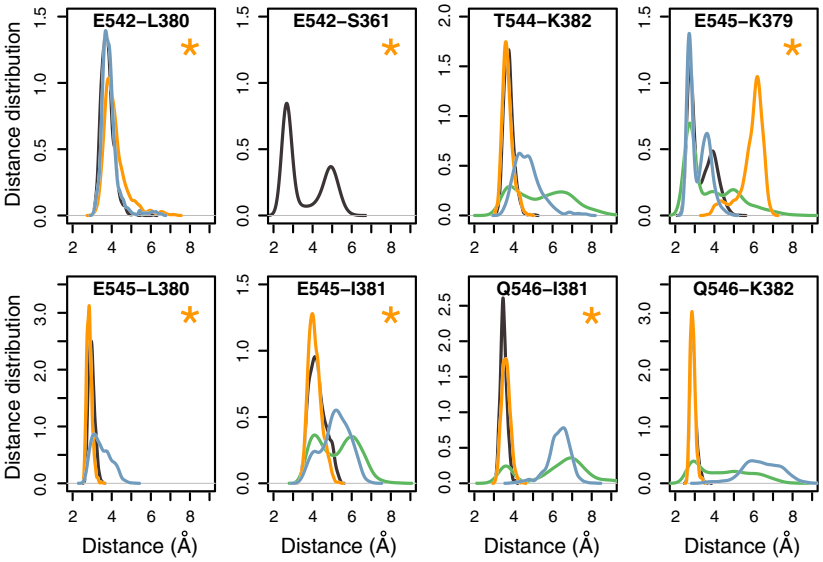

Fig. 3. Stabilizing interactions at the nSH2–helical domain interface: probability distribution of the distance between residues along the MD trajectories (see Experimental procedures). Gray: WT. Orange: E542K/E545K. Blue: N345K. Green: R38C/R88Q. In panels with a star, the distance involves mutated residues.

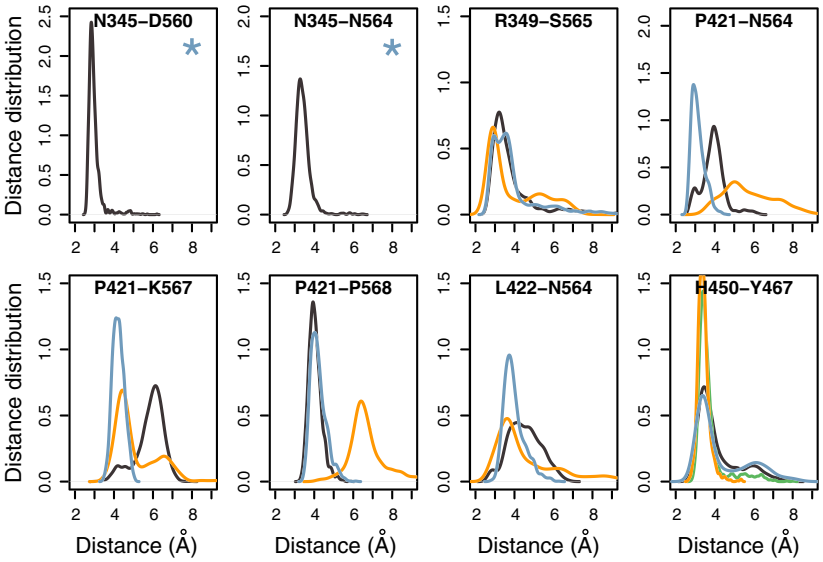

Fig. 4. Stabilizing interactions at the C2–iSH2 domain interface: probability distribution of the distance between residues along the MD trajectories (see Experimental procedures). Gray: WT. Orange: E542K/E545K. Blue: N345K. Green: R38C/R88Q. In panels, with a star the distance involves mutated residues.

between the ABD and the iSH2 domain and the p110α core, as suggested in [35]. The other mutants do not show significant changes in these interactions (Fig. 5). Consequently, the R38C and R88Q mutations disrupt all three interfaces considered, whereas the E542K/E545K and N345K mutations only disrupt the nSH2–helical and C2–iSH2 interfaces. This suggests that the localized structural and dynamic changes induced by the R38C/R88Q mutation are transmitted to the nSH2 domain through the rigid coiled-coil iSH2 domain. These changes reduce the autoinhibitory interaction between the nSH2 domain and p110α.

Oncogenic mutations increase the conformational heterogeneity of p85α

To further characterize the dynamic effects of the studied oncogenic mutations, we computed the solvent-accessible surface area (SASA) for all residues of p85α, as a function of time. First, we identified all of the nSH2 residues that are buried in the WT by defining a cutoff of the normalized SASA (nSASA) of < 0.2 (see Experimental procedures). We determined that those residues become more exposed upon mutations in the helical (E542K/E545K) and C2 (N345K) domains (Fig. 6A), as shown by the increased probability of a higher nSASA. Similarly, comparison of the nSASA of

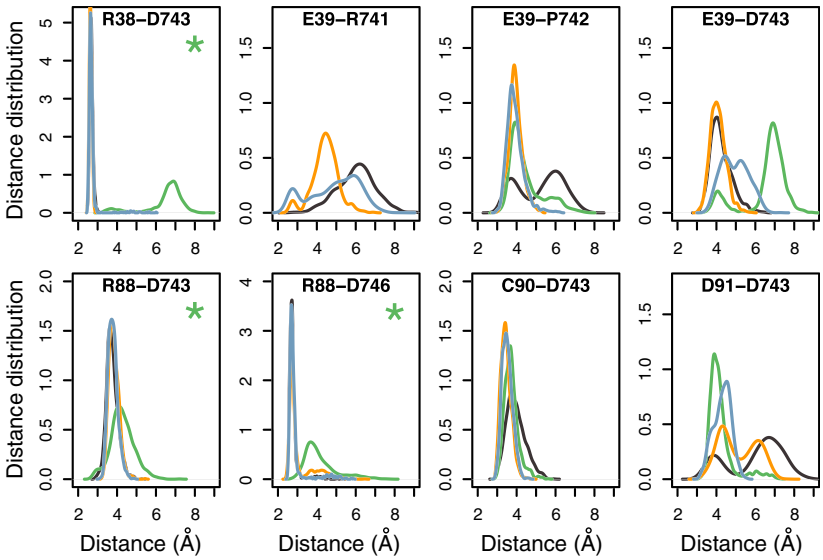

Fig. 5. Stabilizing interactions at the ABD–kinase domain interface. Gray: WT. Orange: E542K/E545K. Blue: N345K. Green: R38C–R88Q. In panels with a star, the distance involves mutated residues.

buried residues in the iSH2 domain showed that these residues become more exposed to solvent in all of the mutants (Fig. 6B).

Among the nSH2 domain residues that become more exposed upon mutation are residues 344–346, located in the helix at the interface of the C2, iSH2 and nSH2 domains. The nSASAs of these residues show large variations over time, especially in the N345K C2 mutant. Residue 369, located in the interface between the helical and nSH2 domains and facing the loop where the E542K/E545K mutation is located, becomes slightly more exposed in the helical domain mutant, but not in the other mutants. The nSASA of residues 414–420, located in a loop facing the helical domain, also shows large fluctuations, suggesting that the nSH2 domain undergoes larger fluctuations in the mutants.

In the iSH2 domain, residues 481, 564 and 568, located at the C2–iSH2 interface, have, on average, larger nSASAs in the mutants than in the WT (data not shown). Residues 574–577 and 447–454, which are present in the helices of the coiled-coil iSH2 domain facing the nSH2 domain, show either larger nSASAs or larger fluctuations in the nSASA in the mutants

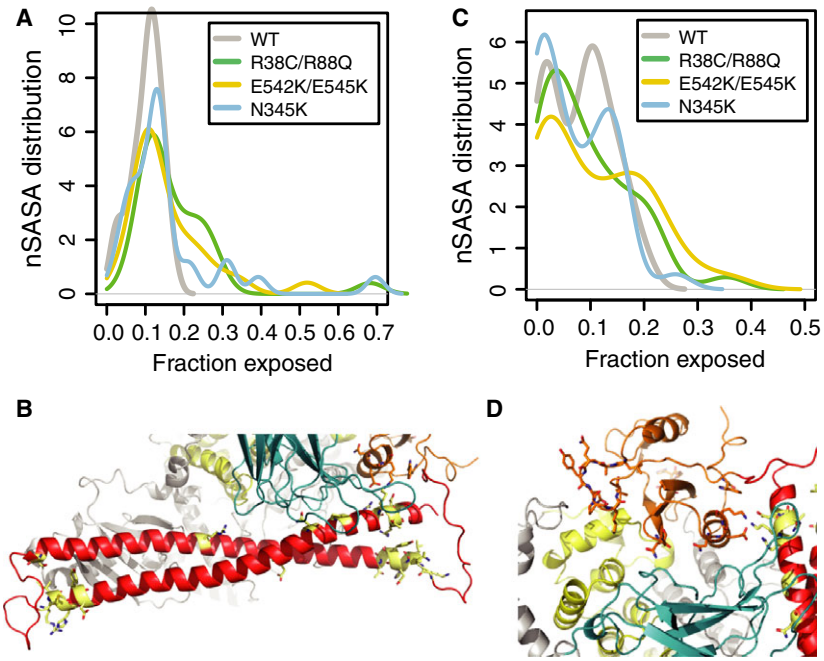

Fig. 6. nSASA of the nSH2 and iSH2 residues. (A) nSASA probability distribution for residues at the interface between the helical and nSH2 domains. (B) Ribbon representation of the p85α-helical domain interface. Residues shown as yellow sticks are those for which we measured large changes in the nSASA with respect to the WT. (C) nSASA probability distribution for residues at the interface between p110α and the iSH2 domain. (D) Ribbon representation of the p110α–iSH2 interface. Residues shown as yellow sticks are those for which we measured large changes in the nSASA with respect to the WT. The domain color coding is the same as in Fig. 1.

than in the WT. Similarly, residues 505 and 523–526, which are present at the interface between the iSH2 domain and the ABD, also show larger fluctuations in the mutants. These results suggest that mutations in all three interfaces studied have a significant effect on the dynamics of the iSH2 domain.

Oncogenic mutations lead to PI3Kα activation by releasing the p85α nSH2 inhibitory effect

Figure 7 shows the model proposed for the effects of the studied oncogenic mutations and how they contribute to PI3Kα activation [18]. In the WT, the p85α nSH2 domain has an autoinhibitory effect on PI3Kα activity (Fig. 7A). The studied mutations E542K/E545K, R38C/R88Q and N345K are located at interfaces between the helical and nSH2 domains, the C2 and iSH2 domains, and ABD and the kinase domain (Fig. 7B). The E542K and E545K mutations are located in the loop region of the helical domain that contacts the nSH2 domain (Fig. 7B). Structural studies have shown that these residues interact with Lys379 and Arg340 of the nSH2 domain [16], 'locking' the inhibited conformation of PI3Kα. Therefore, to bind the phosphorylated tyrosine-containing loop of the effector protein, the nSH2 domain must spend part of the time away from its inhibitory position (Fig. 7C). The C2 domain and ABD mutations increase this effect by weakening the interaction between the helical and nSH2 domains, and allowing the nSH2 domain to spend a larger fraction of the time away from the helical domain, resulting in PI3Kα activation. These results were observed in the ENM and MD simulations: the ENM showed that the mutants' nSH2 domains undergoe larger fluctuations, suggesting an increase in positional heterogeneity; MD simulations showed that all of the mutations weaken the interdomain interactions at the nSH2–helical interface, where residues also undergo larger fluctuations in the nSASA.

We also observed that the mutations examined have significant effects on the domain–domain interactions at the C2–iSH2 interface, and that, for all mutants, the iSH2 domain has increased positional heterogeneity (Fig. 7D). This is reflected in the increase in nSASA fluctuations shown by residues located at the p110α–p85α interface. The ABD–kinase domain interface is only weakened by mutations in the ABD. However, the the nSASA of residues at the interface between the ABD, kinase domain and iSH2 domain also shows larger fluctuations in the mutants than in the WT. These results support the proposed mechanism whereby, given the rigidity of the coiled-coil, the iSH2 domain acts as a rod that transmits the conformational and dynamic effects of the different mutations throughout the protein [18]. The proposed mechanism explains how mutations that are so far away from the nSH2 domain can still act by relieving nSH2 inhibition. Moreover, this mechanism exemplifies how the activation of PI3Kα corresponds to

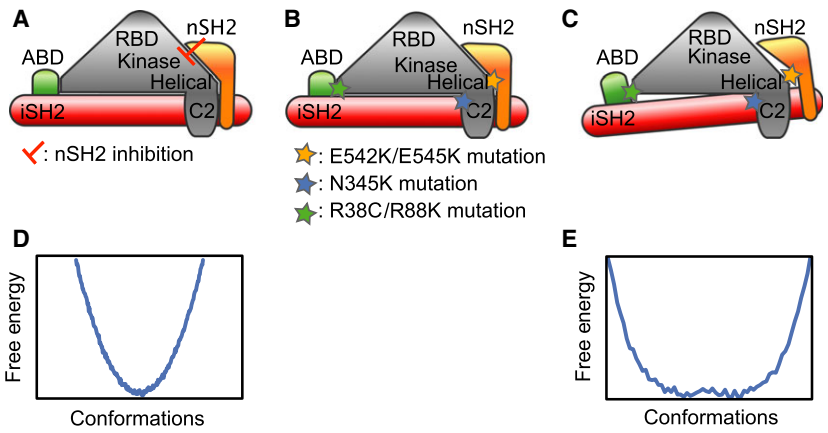

Fig. 7. Schematic representation of the mechanism of activation by oncogenic mutations at domain interfaces. (A) Physiological activation of PI3Kα represents reversal of autoinhibition by the nSH2 domain. (B) The studied oncogenic mutations are located at the nSH2-helical domain, C2–iSH2 domain and ABD–kinase domain interfaces. (C) All studied mutations effectively weaken the nSH2–helical domain and the C2–iSH2 domain interfaces [18]. (D) Schematic free energy profile showing that, in the WT, the p110α nSH2 domain has a small set of well-defined conformations which, given an appropriate reaction coordinate, can be represented by a free-energy profile with a single well. In these conformations, the nSH2 domain inhibits the activity of PI3Kα. (E) Oncogenic mutations change the dynamics of the nSH2 domain. In these cases, the average conformation is the same, but now the nSH2 domain shows greater positional heterogeneity. As a result, the inhibitory conformation is less abundant.

allosteric activation: changes in stability between different components of the system induce structural rearrangements [29,30,36]. Here, changes in protein dynamics, especially those attributable to destabilization of the p110α–p85α interaction, result in allosteric communication between distant sites of the protein that increase the population of the kinase active conformations [37–39].

In its resting state, PI3Kα is autoinhibited by the interaction of a loop of the helical domain of p110α with a groove in the nSH2 domain of p85α [40,41]. Despite this inhibition, the enzyme has significant basal activity [10]. Activation of PI3Kα by its physiological effectors – the phosphotyrosine (pTyr) of an activated RTK or of an RTK substrate – results in a modest two-fold to four-fold increase in the rate of the reaction [10,40]. Activation is the result of pTyr binding to the same groove of the nSH2 domain as the helical domain loop, dislodging the nSH2 domain from its inhibitory position. For the pTyr to have access to bind to the nSH2 groove, the groove must be empty at least part of the time, indicating a dynamic interaction. The fraction of the time that the nSH2 domain spends away from its inhibitory position may account for the PI3Kα basal activity. All of these considerations point to a highly dynamic autoinhibited ground state that can access, through fluctuations, noninhibited states of highly similar energies.

To date, the coordinates of 11 structures of large PI3Kα fragments have been deposited in the Protein Data Bank (PDB) [15,16,40–43], including five reported by us [15,16,41]. The proteins were crystallized under different conditions in several different crystal forms with different crystal contacts. Nevertheless, the rmsd for > 870 aligned α carbons varies only between 0.55 Å and 0.98 Å. In some of the structures, the density for the nSH2 domain was reported to be weak, indicating positional disorder for this p85α domain. In addition, some of the largest deviations were observed at the ends of the iSH2 coiled-coil. These observations can be interpreted as indicating that the nSH2 domain and the ends of the iSH2 domain are conformationally less constrained than the p110α domains. Nevertheless, one area of p110α shows conformational heterogeneity: in most of the structures, no density is observed for the activation loop (residues 933–957 of p110α). When it is observed in the structures of these and other kinases, it adopts different conformations [40,41]. This is particularly important, because a particular conformation of this loop is one of the determinants of activation of the enzyme [37,41]. These local diverse conformations – those of the activation loop and those reflecting weak interactions between p110α and p85α – do not amount to a defined global conformational change, but rather to dynamically accessible local conformations [44]. We propose that oncogenic mutations in the ABD and the C2 domain exert their activation effect by weakening the interactions that modulate the dynamics of the global motions of the nSH2 and iSH2 domains, including the position of the nSH2 domain relative to the rest of the molecule. Mutations at positions 542 and 545 do this directly by disrupting the quaternary interaction between the nSH2 and helical domains [40]. For example, if, for simplicity, we assume that the energetics of the motions of the nSH2 domain along a coordinate that changes its interaction with the helical domain are approximated by a harmonic potential, i.e.

$$P(x) = \exp -[1/2k \cdot (x - x_0)^2]$$

where $P(x)$ is the probability of adopting the position x away from the equilibrium position x_0, and k is the force-restoring constant, we can estimate the effect of weakening the interactions of the nSH2 domain with p110α. For a state that is, for example, 1.5 Å from the ground state, if the value of an originally soft constant of 2 kcal/Å^2 is changed to a softer constant (1 kcal·Å^{-2}), the probability of the state increases by a factor of > 3 without a change in the structure of the ground state (Fig. 7D,E). A simple weakening of the interaction between p110α and p85α can by itself explain the levels of activation observed in PI3Kα.

Visualization of the active site sheds light on the effects of these changes on the activation of PI3Kα. For example, Fig. 8B,C shows the conformation of the kinase activation loop of the WT and that of the E542K/E545K mutant. Figure 8A shows that the activation loop in the WT MD simulations has a conformation that resembles that of the crystal structure, which is locked in the inactive conformation by interactions between the activation loop and the iSH2 domain. In contrast, in the simulation of the E542K/E545K mutant, the interaction between the iSH2 domain and the activation loop is disrupted, displacing the activation loop from the iSH2 domain. Further research should address how these changes relate to the active conformation of the activation loop.

Discussion

We investigated the effects of five p110α oncogenic mutations on the conformational heterogeneity and dynamics of PI3Kα by using different computational methods. Experimental evidence has linked all of these oncogenic mutations to gain of enzymatic activity. We

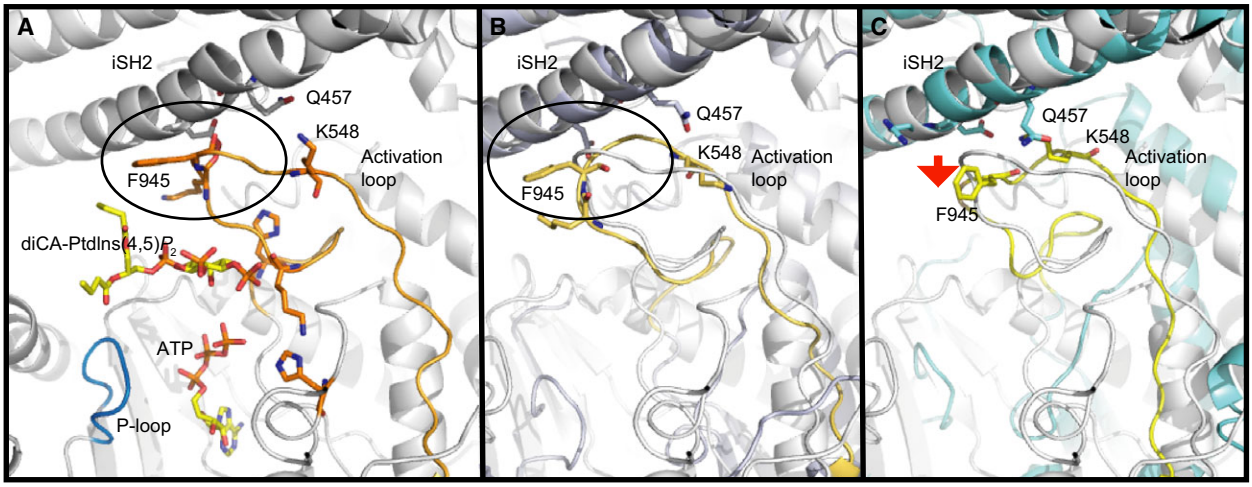

Fig. 8. Structural insights into the active site. (A) Model of the active site based on the alignment of the crystal structures of PI3Kα in complex with its lipid substrate, diC4–phosphoinositol-4,5-bisphosphate [PtdIns(4,5)P_2] (PDB ID 4OVV) and the p110α–ATP complex (PDB ID 1E8X). In the active site, the binding site for the lipid substrate (yellow) is adjacent to the ATP-binding site, which is located between the P-loop (residues 772–778 of p110α), the activation loop (residues 933–957 of p110α), and the p85α iSH2 domain. In this model, the activation loop is locked into the inactive conformation by stacking interactions between Phe945 (p110α) and Leu598 (p85α), and between Lys948 (p110α) and Gln591 (p85α). (B) The most representative structure obtained from the WT MD simulations (colored). The model described in (A) is shown in gray. In this conformation, the activation loop adopts a similar structure to the one shown in (A), locked in the inactive conformations. (C) The most representative structure obtained from the E542K/E545K mutant MD simulations (colored). The model described in (A) is shown in gray. This conformation shows how, in the mutant, the interactions between the iSH2 domain and the activation loop are disrupted, and the activation loop is displaced from the iSH2 domain.

explored the hypothesis that gain of enzymatic activity is brought about by the local increase in the populations of PI3Kα with larger separation in the inhibitory interface between the p110α helical domain and the p85α nSH2 domain. As a consequence, the relative occupancies of the active and inactive conformations of the kinase domain are shifted, making the activate conformation more populated in the mutated PI3Kα. Overall, we observe that all oncogenic mutations weaken the p110α–p85α interactions, at both the nSH2 and the iSH2 interfaces, which results in higher positional heterogeneity of the nSH2 domain. This was shown in ENM calculations by the changes in the fluctuation profiles of the nSH2 domains of the mutants as compared with those of the WT. Closer examination of these profiles reveals that, in all studied mutants, the nSH2 region that faces the helical domain shows increased positional heterogeneity. Furthermore, by analyzing the changes in the SASA obtained from MD simulations, we determined that residues located at the interface between the nSH2 and helical domains become more exposed in the mutants, in agreement with the HDX-MS data [22]. Most importantly, these changes were observed even when the mutations were located distant from the nSH2–helical interface. Finally, analysis of the molecular contacts between residues at the p110α–p85α interface shows the different effects of the different studied oncogenic mutants. For example, some of the stabilizing contacts between the helical and nSH2 domains and the C2 and iSH2 domains are lost in all of the mutants, suggesting that the overall effect of the oncogenic mutations is to increase the conformational heterogeneity of the PI3Kα dimer. The stabilizing contacts between the ABD and the iSH2 domain were only weakened in the R38C/R88Q mutant.

In summary, our studies shed light on the mechanism by which some oncogenic mutations found in different PI3Kα domains may lead to constitutively active enzymes. As described, oncogenic mutations at the allosteric sites destabilize the p110α–p85α dimer, shifting the nSH2 domain from being mostly in its autoinhibitory conformation to being an ensemble of conformations with higher conformational heterogeneity, in which the noninhibited conformations are more abundant. This allosteric change in the conformation of the nSH2 domain changes the relative stabilities of the active and inactive conformations of the kinase domain, making the active conformation more accessible. It remains to be determined how these dynamic changes affect the conformational heterogeneity of the activation and catalytic loops in the kinase domain,

and how this is linked to constitutive activation of PI3Kα. We propose that the observed dynamic changes shift the relative occupancies of the active and inactive conformations of the kinase domain, making the active conformation more abundant in the mutant PI3Kαs. This system exemplifies a case of allostery, whereby changes in the thermal fluctuations resulting from destabilization of its dimeric state result in increased enzymatic activity. This mechanism may apply to other enzymes and/or macromolecular complexes that play a key role in cell signaling [39,45].

From a modeling perspective, we have shown that, when large multimeric proteins or macromolecular complexes are studied, different computational approaches have different strengths, and that a comprehensive approach can provide new insights for answering biologically relevant questions. We used ENMs to obtain significant dynamic information by focusing on the general movements present in a subset (i.e. a low-frequency subset) of normal modes rather than characterizing individual modes. This was accomplished by generating random linear combinations of displacement vectors of atoms to study the flexibility of different domains of the protein. Even though the results of these combinations do not necessarily represent the actual movements of the protein, they are useful tools for assessing the flexibility of different regions of the molecule. MD simulations, on the other hand, provided detailed information about the molecular contacts that define the stability of the p110α–p85α dimer.

Experimental procedures

Initial models

The crystallographic structures of WT p110α in complex with the iSH2 domain of p85α [15] (PDB accession code 2RD0) and the H1047R mutant of p110α in complex with the niSH2 domain of p85α [16] (PDB accession code 3HIZ) were used to build the different models. Related structures of the free WT and the WT in complex with the lipid substrate have been recently published (PDB accession code 4OVU) [41]. All crystal structures lack some loop regions, which were built with the loop-building option of MODELLER 9v8 [46]. One loop of critical importance that needed to be modeled was the activation loop (p110α residues 933–957). This loop was modeled in the inactive conformation with the activation loop of the PI3Kβ isoform as a template [47]. We modeled the WT and five mutants of p110α in complex with the nSH2 and iSH2 domains of p85α. Starting with the WT model, each mutant was modeled *in silico* with MODELLER 9v8 [46]. We studied the helical domain mutations E542R/E545R and E542K/E545K, the ABD mutations R38C/R88Q and R38D/R88D, and the C2 domain mutation N345K. In the models of the helical and ABD mutants, we combined both commonly observed mutations to enhance the structural and dynamic effects observed with computational methods.

The potential energy of each of these structures was minimized by use of the program NAMD with the CHARMM27/CMAP force field [48,49], with the conjugate gradient and adapted basis Newton–Raphson method algorithms. After minimization, each of these models was used for NMA and MD simulations.

ENMs

Internal motions of proteins are important for their biological function, especially large-amplitude (and/or low-frequency) motions that may be necessary for activation or for allosteric transitions. NMA has been shown to be a successful and direct method for identifying these large-amplitude motions [50,51]. In general terms, NMA is the study of coupled harmonic potential wells by analytical means [33,52]. In particular, we focused on the NMA of coarse-grained ENMs of the WT and mutant PI3Kαs. Low-frequency modes obtained with this method have been shown to correspond to the wide conformational fluctuations observed experimentally around a given stable conformation [53–55].

Starting from a stable structure of a protein, which is assumed to be a minimum of the potential energy surface, a harmonic approximation is used to calculate vibrations around this minimum. In this model, each residue of the protein is represented by the Cα, and the springs connecting the nodes represent the bonded and nonbonded interactions between the pairs of residues that are within a distance range defined by a cutoff r_c. Furthermore, in this representation it is assumed that the fluctuations are isotropic and Gaussian, such that the conformational potential, for a system of N residues, is given by:

$$V = \frac{\gamma}{2}\left[\sum_{i,j}^{N}[(\Delta X_i - \Delta X_j)^2 + (\Delta Y_i - \Delta Y_j)^2 + (\Delta Z_i - \Delta Z_j)^2]\right] \quad (1)$$

where γ is a single force constant and ΔX_i, ΔY_i and ΔZ_i are the N-dimensional vectors whose elements are the fluctuations of residue i. To perform the NMA, it is necessary to diagonalize the Hessian matrix, whose elements are the second derivative of the potential energy with respect to the coordinates (Eqn 1). As a result, one obtains a set of orthonormal basis vectors that describe the N-dimensional configurational space of the protein.

Structural analysis of the normal modes

To characterize the dynamic effects of the mutations, we analyzed the eigenvectors obtained by NMA for every PI3Kα model. Every eigenvector $\Delta R_k(i)$ is normalized such that:

$$\sum_{k=1}^{N} \Delta R_k(i)^2 = 1 \quad (2)$$

where k indicates the normal mode and i identifies the residue in the structure. The set of the $N - 1$ eigenvectors form an orthogonal basis ($\Delta \boldsymbol{R_K} \cdot \Delta \boldsymbol{R_l} = 0$ for $k \neq l$) that can be used to model the configurational space of the protein near the initial conformation. Previous studies have shown that functional movements associated with conformational changes are encoded in low-frequency modes [50,51,56].

We investigated the fluctuations of each of the protein's domains by analyzing the information encoded in the eigenvectors. For example, for residues i_n to i_m, the sum

$$s = \sum_{i=i_n}^{i_m} \Delta R_k(i)$$

can be interpreted as the contributions of the segment between residues i_n and i_m to the motion described by the kth eigenvector.

As comparing individual normal modes may not provide straightforward information, we generated random linear combinations of the first six vibrational normal modes for different domains. We computed the fluctuations vector ($\boldsymbol{q}$) by first extracting from the kth eigenvector the portion of the normal mode that corresponds to the domain (d) being studied (ΔR_k^d), and then generating the linear combination as:

$$q = \sum_{k=1}^{6} \alpha_k \Delta R_k^d \quad (3)$$

where the coefficient α correspond to random numbers that satisfy the condition

$$\sum_k \alpha_k = 1$$

We determined that 500 linear combinations

$$q_{\text{final}} = \sum_{m=1}^{500} q_m$$

are sufficient to obtain convergent fluctuation profiles for the protein's domains. We compared fluctuation profiles of the WT with those of the mutants.

MD simulations

Explicit solvent simulations were carried out with NAMD 2.9 [57], the CHARMM27/CMAP force field [58,59], and the TIP3P water model. The initial models were solvated in a box of water molecules of dimensions 125 × 117 × 102 Å. The system was minimized with, first, the conjugate gradient and adapted basis Newton–Raphson methods, for 4000 steps in each case. The system was then gradually heated from 100 K to 300 K over a 4-ns simulation, and this was followed by equilibration at 300 K (for 2 ns) in the NPT ensemble. Periodic boundary conditions were used in all of our calculations, and long-range electrostatics were treated with the particle mesh Ewald method [60]. The cutoff distance for nonbonded Coulomb and Lennard–Jones interactions was set to a 12 Å cutoff, with a switching function at 10 Å. Simulations were carried out with an integration time step of 2 fs by use of the SETTLE algorithm, while keeping all bonds to hydrogen atoms rigid. Production simulations were performed at a constant temperature (of 310 K) and pressure by use of Langevin dynamics. Production runs were 50 ns in length. For analysis, we considered the last 40 ns of each production run.

Structural analysis of the MD simulations

To identify interdomain contacts at the interface between subunits, two residues were considered to be in contact if the distance between their Cβs (Cα for glycine) was shorter than 9 Å. The dynamics of each interaction were estimated by recording the smallest distance between heavy atoms within every 20-ps timeframe along each trajectory. The SASA for all residues of p85α was calculated with NACCESS [61], which was modified to read different frames of the trajectory and measure the SASA per residue as a function of simulation time. A probe of 1.4 Å was used. We defined the nSASA as the measured SASA divided by the maximum possible SASA for each residue [62], such that the nSASA ranges between 0 and 1.

Acknowledgements

This work was supported by the National Institute of Health (NIH grant CA-43460) and the National Science Foundation (NSF grant MCB-0450465). Computational resources were provided by the Extreme Science and Engineering Discovery Environment (XSEDE), which is supported by the National Science Foundation (grant numbers MCB110058 and MCB130213).

Competing interests

The authors declare no competing interests.

Author contributions

I. Echeverria, S. B. Gabelli and L. M. Amzel designed the research. I. Echeverria, Y. Liu and L. M. Amzel

performed research and analyzed the data. I. Echeverria, S. B. Gabelli and L.M. Amzel wrote the paper.

References

1 Fyffe C, Buus R & Falasca M (2013) Genetic and epigenetic regulation of phosphoinositide 3-kinase isoforms. *Curr Pharm Des* **19**, 680–686.
2 Cantley LC (2002) The phosphoinositide 3-kinase pathway. *Science* **296**, 1655–1657.
3 Cully M, You H, Levine AJ & Mak TW (2006) Beyond PTEN mutations: the PI3K pathway as an integrator of multiple inputs during tumorigenesis. *Nat Rev Cancer* **6**, 184–192.
4 Katso R, Okkenhaug K, Ahmadi K, White S, Timms J & Waterfield MD (2001) Cellular function of phosphoinositide 3-kinases: implications for development, immunity, homeostasis, and cancer. *Annu Rev Cell Dev Biol* **17**, 615–675.
5 Geering B, Cutillas PR, Nock G, Gharbi SI & Vanhaesebroeck B (2007) Class IA phosphoinositide 3-kinases are obligate p85-p110 heterodimers. *Proc Natl Acad Sci USA* **104**, 7809–7814.
6 Shepherd PR, Siddle K & Navé BT (1997) Is stimulation of class-1 phosphatidylinositol 3-kinase activity by insulin sufficient to activate pathways involved in glucose metabolism. *Biochem Soc Trans* **25**, 978–981.
7 Forbes SA, Bindal N, Bamford S, Cole C, Kok CY, Beare D, Jia M, Shepherd R, Leung K, Menzies A *et al.* (2010) COSMIC: mining complete cancer genomes in the Catalogue of Somatic Mutations in Cancer. *Nucleic Acids Res* **39**, D945–D950.
8 Samuels Y, Wang Z, Bardelli A, Silliman N, Ptak J, Szabo S, Yan H, Gazdar A, Powell SM, Riggins GJ *et al.* (2004) High frequency of mutations of the PIK3CA gene in human cancers. *Science* **304**, 554.
9 Samuels Y & Waldman T (2011) Oncogenic Mutations of PIK3CA in Human Cancers. Phosphoinositide 3-kinase in Health and Disease, pp. 21–41. Springer, Berlin, Heidelberg.
10 Carson JD, Van Aller G, Lehr R, Sinnamon RH, Kirkpatrick RB, Auger KR, Dhanak D, Copeland RA, Gontarek RR, Tummino PJ *et al.* (2008) Effects of oncogenic p110alpha subunit mutations on the lipid kinase activity of phosphoinositide 3-kinase. *Biochem J* **409**, 519–524.
11 Chaussade C, Cho K, Mawson C, Rewcastle GW & Shepherd PR (2009) Functional differences between two classes of oncogenic mutation in the PIK3CA gene. *Biochem Biophys Res Commun* **381**, 577–581.
12 Bachman KE, Argani P, Samuels Y, Silliman N, Ptak J, Szabo S, Konishi H, Karakas B, Blair BG, Lin C *et al.* (2004) The PIK3CA gene is mutated with high frequency in human breast cancers. *Cancer Biol Ther* **3**, 772–775.
13 Broderick DK, Di C, Parrett TJ, Samuels YR, Cummins JM, McLendon RE, Fults DW, Velculescu VE, Bigner DD & Yan H (2004) Mutations of PIK3CA in anaplastic oligodendrogliomas, high-grade astrocytomas, and medulloblastomas. *Cancer Res* **64**, 5048–5050.
14 Rudd ML, Price JC, Fogoros S, Godwin AK, Sgroi DC, Merino MJ & Bell DW (2011) A unique spectrum of somatic PIK3CA (p110alpha) mutations within primary endometrial carcinomas. *Clin Cancer Res* **17**, 1331–1340.
15 Huang C-H, Mandelker D, Schmidt-Kittler O, Samuels Y, Velculescu VE, Kinzler KW, Vogelstein B, Gabelli SB & Amzel LM (2007) The structure of a human p110alpha/p85alpha complex elucidates the effects of oncogenic PI3Kalpha mutations. *Science* **318**, 1744–1748.
16 Mandelker D, Gabelli SB, Schmidt-Kittler O, Zhu J, Cheong I, Huang C-H, Kinzler KW, Vogelstein B & Amzel LM (2009) A frequent kinase domain mutation that changes the interaction between PI3Kalpha and the membrane. *Proc Natl Acad Sci USA* **106**, 16996–17001.
17 Zhao L & Vogt PK (2008) Helical domain and kinase domain mutations in p110alpha of phosphatidylinositol 3-kinase induce gain of function by different mechanisms. *Proc Natl Acad Sci USA* **105**, 2652–2657.
18 Gabelli SB, Echeverria I, Alexander M, Duong-Ly KC, Chaves-Moreira D, Brower ET, Vogelstein B & Amzel LM (2014) Activation of PI3Kα by physiological effectors and by oncogenic mutations: structural and dynamic effects. *Biophys Rev* **6**, 89–95.
19 Burke JE, Vadas O, Berndt A, Finegan T, Perisic O & Williams RL (2011) Dynamics of the phosphoinositide 3-kinase p110δ interaction with p85α and membranes reveals aspects of regulation distinct from p110α. *Structure* **19**, 1127–1137.
20 Gkeka P, Evangelidis T, Pavlaki M, Lazani V, Christoforidis S, Agianian B & Cournia Z (2014) Investigating the structure and dynamics of the PIK3CA wild-type and H1047R oncogenic mutant. *PLoS Comput Biol* **10**, e1003895.
21 Gymnopoulos M, Elsliger M-A & Vogt PK (2007) Rare cancer-specific mutations in PIK3CA show gain of function. *Proc Natl Acad Sci USA* **104**, 5569–5574.
22 Burke JE, Perisic O, Masson GR, Vadas O & Williams RL (2012) Oncogenic mutations mimic and enhance dynamic events in the natural activation of phosphoinositide 3-kinase p110α (PIK3CA). *Proc Natl Acad Sci USA* **109**, 15259–15264.
23 Engelman JA, Chen L, Tan X, Crosby K, Guimaraes AR, Upadhyay R, Maira M, McNamara K, Perera SA, Song Y *et al.* (2008) Effective use of PI3K and MEK

inhibitors to treat mutant Kras G12D and PIK3CA H1047R murine lung cancers. *Nat Med* **14**, 1351–1356.
24 Bauer TM, Patel MR & Infante JR (2014) Targeting PI3 kinase in cancer. *Pharmacol Ther* **146**, 53–60.
25 Porta C, Paglino C & Mosca A (2014) Targeting PI3K/Akt/mTOR Signaling in Cancer. *Front Oncol* **4**, 64.
26 Zheng Z, Amran SI, Thompson PE & Jennings IG (2011) Isoform-selective inhibition of phosphoinositide 3-kinase: identification of a new region of nonconserved amino acids critical for p110α inhibition. *Mol Pharmacol* **80**, 657–664.
27 Gabelli SB, Mandelker D, Schmidt-Kittler O, Vogelstein B & Amzel LM (2010) Somatic mutations in PI3Kalpha: structural basis for enzyme activation and drug design. *Biochim Biophys Acta* **1804**, 533–540.
28 Vadas O, Burke JE, Zhang X, Berndt A & Williams RL (2011) Structural basis for activation and inhibition of class I phosphoinositide 3-kinases. *Sci Signal* **4**, re2.
29 Cooper A & Dryden DTF (1984) Allostery without conformational change. *Eur Biophys J* **11**, 103–109.
30 Motlagh HN, Wrabl JO, Li J & Hilser VJ (2014) The ensemble nature of allostery. *Nature* **508**, 331–339.
31 Tsai C-J, Del Sol A & Nussinov R (2009) Protein allostery, signal transmission and dynamics: a classification scheme of allosteric mechanisms. *Mol BioSyst* **5**, 207–216.
32 Nussinov R & Ma B (2012) Protein dynamics and conformational selection in bidirectional signal transduction. *BMC Biol* **10**, 2.
33 Bahar I & Rader AJ (2005) Coarse-grained normal mode analysis in structural biology. *Curr Opin Struct Biol* **15**, 586–592.
34 Wu H, Shekar SC, Flinn RJ, El-Sibai M, Jaiswal BS, Sen KI, Janakiraman V, Seshagiri S, Gerfen GJ, Girvin ME *et al.* (2009) Regulation of Class IA PI 3-kinases: C2 domain-iSH2 domain contacts inhibit p85/p110alpha and are disrupted in oncogenic p85 mutants. *Proc Natl Acad Sci USA* **106**, 20258–20263.
35 Miled N, Yan Y, Hon W-C, Perisic O, Zvelebil M, Inbar Y, Schneidman-Duhovny D, Wolfson HJ, Backer JM & Williams RL (2007) Mechanism of two classes of cancer mutations in the phosphoinositide 3-kinase catalytic subunit. *Science* **317**, 239–242.
36 Blacklock K & Verkhivker GM (2014) Computational modeling of allosteric regulation in the Hsp90 chaperones: a statistical ensemble analysis of protein structure networks and allosteric communications. *PLoS Comput Biol* **10**, e1003679.
37 Tsai C-J, Del Sol A & Nussinov R (2008) Allostery: absence of a change in shape does not imply that allostery is not at play. *J Mol Biol* **378**, 1–11.
38 Weinkam P, Chen YC, Pons J & Sali A (2013) Impact of mutations on the allosteric conformational equilibrium. *J Mol Biol* **425**, 647–661.
39 Nussinov R & Tsai C-J (2015) Allostery without a conformational change? Revisiting the paradigm. *Curr Opin Struct Biol* **30**, 17–24.
40 Hon W-C, Berndt A & Williams RL (2012) Regulation of lipid binding underlies the activation mechanism of class IA PI3-kinases. *Oncogene* **31**, 3655–3666.
41 Miller MS, Schmidt-Kittler O, Bolduc DM, Brower ET, Chaves-Moreira D, Allaire M, Kinzler KW, Jennings IG, Thompson PE, Cole PA *et al.* (2014) Structural basis of nSH2 regulation and lipid binding in PI3Kα. *Oncotarget* **5**, 5198–5208.
42 Zhao Y, Zhang X, Chen Y, Lu S, Peng Y, Wang X, Guo C, Zhou A, Zhang J, Luo Y *et al.* (2013) Crystal structures of PI3Kα complexed with PI103 and its derivatives: new directions for inhibitors design. *ACS Med Chem Lett* **5**, 138–142.
43 Furet P, Guagnano V, Fairhurst RA, Imbach-Weese P, Bruce I, Knapp M, Fritsch C, Blasco F, Blanz J, Aichholz R *et al.* (2013) Discovery of NVP-BYL719 a potent and selective phosphatidylinositol-3 kinase alpha inhibitor selected for clinical evaluation. *Bioorg Med Chem Lett* **23**, 3741–3748.
44 Popovych N, Sun S, Ebright RH & Kalodimos CG (2006) Dynamically driven protein allostery. *Nat Struct Mol Biol* **13**, 831–838.
45 Tsai C-J & Nussinov R (2014) A unified view of "how allostery works". *PLoS Comput Biol* **10**, e1003394.
46 Fiser A & Sali A (2003) Modeller: generation and refinement of homology-based protein structure models. *Meth Enzymol* **374**, 461–491.
47 Zhang X, Vadas O, Perisic O, Anderson KE, Clark J, Hawkins PT, Stephens LR & Williams RL (2011) Structure of lipid kinase p110β/p85β elucidates an unusual SH2-domain-mediated inhibitory mechanism. *Mol Cell* **41**, 567–578.
48 Brooks BR, Bruccoleri RE, Olafson BD, States DJ, Swaminathan S & Karplus M (1983) CHARMM: A program for macromolecular energy, minimization, and dynamics calculations. *J Comput Chem* **4**, 187–217.
49 Brooks BR, Brooks CL, MacKerell AD, Nilsson L, Petrella RJ, Roux B, Won Y, Archontis G, Bartels C, Boresch S *et al.* (2009) CHARMM: The biomolecular simulation program. *J Comput Chem* **30**, 1545–1614.
50 Isin B, Schulten K, Tajkhorshid E & Bahar I (2008) Mechanism of signal propagation upon retinal isomerization: insights from molecular dynamics simulations of rhodopsin restrained by normal modes. *Biophys J* **95**, 789–803.
51 Zheng W, Brooks BR & Thirumalai D (2006) Low-frequency normal modes that describe allosteric transitions in biological nanomachines are robust to sequence variations. *Proc Natl Acad Sci USA* **103**, 7664–7669.

52 Bahar I, Wallqvist A, Covell DG & Jernigan RL (1998) Correlation between native-state hydrogen exchange and cooperative residue fluctuations from a simple model. *Biochemistry* **37**, 1067–1075.
53 Tama F & Sanejouand YH (2001) Conformational change of proteins arising from normal mode calculations. *Protein Eng* **14**, 1–6.
54 Temiz NA, Meirovitch E & Bahar I (2004) *Escherichia coli* adenylate kinase dynamics: Comparison of elastic network model modes with mode-coupling 15N-NMR relaxation data. *Proteins: Struct, Funct, Bioinf* **57**, 468–480.
55 Vashisth H & Brooks CL (2012) Conformational sampling of maltose-transporter components in cartesian collective variables is governed by the low-frequency normal modes. *J Phys Chem Lett* **3**, 3379–3384.
56 Vashisth H, Skiniotis G & Brooks CL (2012) Using enhanced sampling and structural restraints to refine atomic structures into low-resolution electron microscopy maps. *Structure* **20**, 1453–1462.
57 Phillips JC, Braun R, Wang W, Gumbart J, Tajkhorshid E, Villa E, Chipot C, Skeel RD, Kalé L & Schulten K (2005) Scalable molecular dynamics with NAMD. *J Comput Chem* **26**, 1781–1802.
58 MacKerell AD, Bashford D, Bellott M, Dunbrack RL, Evanseck JD, Field MJ, Fischer S, Gao J, Guo H, Ha S *et al.* (1998) All-atom empirical potential for molecular modeling and dynamics studies of proteins. *J Phys Chem B* **102**, 3586–3616.
59 Mackerell AD, Feig M & Brooks CL (2004) Extending the treatment of backbone energetics in protein force fields: Limitations of gas-phase quantum mechanics in reproducing protein conformational distributions in molecular dynamics simulations. *J Comput Chem* **25**, 1400–1415.
60 Darden T, York D & Pedersen L (1993) Particle mesh Ewald: An N·log(N) method for Ewald sums in large systems. *J Chem Phys* **98**, 10089.
61 Hubbard SJ & Thornton JM (1993) *NACESS* computer program.
62 Samanta U, Bahadur RP & Chakrabarti P (2002) Quantifying the accessible surface area of protein residues in their local environment. *Protein Eng* **15**, 659–667.